FCD SEGMENTATION USING TEXTURE ASYMMETRY OF MR-T1 IMAGES OF THE BRAIN

Felipe P.G. Bergo, Alexandre X. Falcão

LIV, Institute of Computing, UNICAMP
CP 6176 Campinas, SP, 13083-970, Brazil

Clarissa L. Yasuda, Fernando Cendes

Dept. of Neurology, FCM, UNICAMP
CP 6111 Campinas, SP, 13083-970, Brazil

ABSTRACT

Focal cortical dysplasia is the most common malformation in patients with intractable epilepsy. The segmentation of FCD lesions in MR-T1 images of the brain is a crucial step for treatment planning. In this work we present a new FCD segmentation technique based on analysis of texture asymmetry. This technique does not rely on template-based segmentation and is applicable to patients of any age, regardless of anatomic variations. We evaluated the method on 5 patients (aged 11y–51y), and obtained 100% detection rate and coverage of 76.9% of the lesional voxels.

Index Terms— Image Segmentation, Medical diagnosis, Epilepsy, Focal Cortical Dysplasia, Pattern Recognition

1. INTRODUCTION

Focal Cortical Dysplasia (FCD) is a malformation of cortical development that results in abnormal glial elements and disruption of the normal cortical lamination. It was first described by Taylor [1], and it is the most common malformation in patients with intractable epilepsy [2]. FCD is also a common cause of epilepsy in children and young adults [3, 4].

The problem of FCD detection in MRI consists in identifying the approximate locations of the FCD lesions (usually one voxel inside each lesion, or an approximation of the lesion by some kind of marker). The problem of FCD segmentation consists in identifying the precise spatial extent of FCD lesions, by classifying MRI voxels as either healthy or pathological. Solving FCD segmentation implicitly solves FCD detection. Detection and segmentation of FCD lesions are crucial steps in treatment planning [5, 6, 7].

FCD lesions appear as subtle macroscopic features in brain MR images: blurring of the gray-matter/white-matter (GM/WM) transition, localized GM thickening and hyperintense GM signal [3]. In this work we exploit the asymmetry between texture features of lesional voxels and their healthy counterparts in the opposing brain hemisphere to detect and segment FCD lesions.

2. RELATED WORKS

The most common FCD diagnosis method in clinical practice is the straightforward visual inspection of MR images by specialists. The reported detection rate for this technique is 50% [8]. Techniques such as multiplanar reconstruction (MPR) and curvilinear reformatting (CR) increase the detection rate to 100% [8]. Curvilinear reformatting [9] consists of visualizing 3D MR images as curved surfaces that follow the shape of the brain. This technique improves the visibility of FCD lesions over MPR [8] and can be computed automatically without human interaction [10].

Several recent works presented automatic FCD detection methods, with detection rates varying from 53% to 85% [11, 12, 13, 14]. Most of these works focus on detection rather than segmentation. To our knowledge, Colliot et al. [14] is the only work that report segmentation accuracy rate, with a coverage of 73% of the lesional voxels. Some of these works [11, 12, 14] rely on template-based segmentation techniques of the GM, which are often unreliable for children and patients who underwent brain surgery [15, 16].

3. METHOD

Our method works on volumetric MR-T1 images interpolated to an isotropic voxel size of $1.0\,mm^3$, and comprises 6 steps: (i) mid-sagittal plane (MSP) location, (ii) brain segmentation, (iii) CR computation, (iv) feature extraction, (v) voxel classification and (vi) outlier removal.

3.1. MSP Location

We locate the mid-sagittal plane that divides the brain hemispheres using the heuristic minimization search of Bergo et al. [17]. After the plane is found, the volume is rotated such that the MSP becomes orthogonal to the coordinate system.

3.2. Brain Segmentation

We apply the automatic tree pruning technique [18] to segment the brain. Tree pruning does not rely on templates and performs well regardless of age or anatomic variations [17].

3.3. CR computation

The curvilinear reformatting can be encoded as an Euclidian distance transform computed from the brain's border. This distance transform can be efficiently computed by the IFT-EDT [10].

3.4. Feature Extraction

For each voxel p within the brain, we extract a 16×16 planar texture patch $T_1(p)$ tangent to the brain's curvature (as computed by the CR) and centered at p. The gradient vector of the CR distance transform at the voxel's location provides the surface normal. We also extract a symmetric patch $T_2(p)$, located at the reflection of $T_1(p)$ by the MSP. These patches are illustrated by Fig. 1.

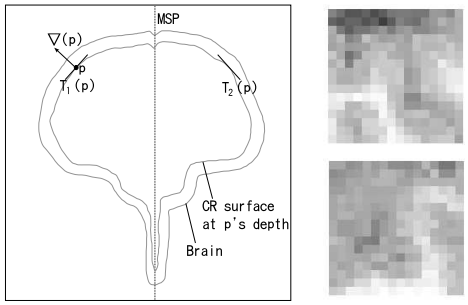

(a) (b)

Fig. 1. Texture patches used for feature extraction: (a) patch location. (b) example of a pair of symmetric patches $T1$ and $T2$.

The patch size was chosen experimentally. Smaller patch sizes did not provide good classification results, while larger patch sizes led to similar results with higher computational cost.

For each patch we compute 6 features: sharpness (h), entropy, homogeneity, contrast, intensity mean (μ) and intensity standard deviation (σ). Sharpness is computed as the sum of pixelwise absolute intensity differences between the patch and a blurred copy of itself obtained by convolution with a 5×5 Gaussian kernel with $\sigma = 7$. Entropy, homogeneity and contrast are computed as presented by Haralick et al. [19], using a 12×12 gray-level cooccurrence matrix. Using these computed values we build a 16-element feature vector associated to voxel p as indicated by Eq. 1. All features are scaled to fit within the $[0, 1]$ interval.

$$fv(p) = \begin{bmatrix} h(T_1(p)) \\ h(T_2(p)) \\ h(T_1(p)) - h(T_2(p)) \\ h(T_1(p))/h(T_2(p)) \\ entropy(T_1(p)) \\ entropy(T_2(p)) \\ contrast(T_1(p)) \\ contrast(T_2(p)) \\ homogeneity(T_1(p)) \\ homogeneity(T_2(p)) \\ \mu(T_1(p)) \\ \mu(T_2(p)) \\ \mu(T_1(p)) - \mu(T_2(p)) \\ \sigma(T_1(p)) \\ \sigma(T_2(p)) \\ \sigma(T_1(p)) - \sigma(T_2(p)) \end{bmatrix} \quad (1)$$

3.5. Voxel Classification

We use a Reduced Coulomb Energy classifier (RCE) [20] to perform the classification of the voxels, based on supervised learning. In the RCE classifier, each training sample becomes a hypersphere in the feature space (in our case, $\mathbb{R}^{16}$). The radius is chosen to be the maximum such that no training sample from a different class is contained in the hypersphere. Classification is performed by testing the test sample for containment within the training samples's hyperspheres. If a test sample falls within an ambiguous space (being contained by hyperspheres of different classes), we classify it as lesional. This is a design decision to prevent false negatives.

3.6. Outlier Removal

The classification result leads to outliers both in lesional and healthy regions. However, the density of voxels classified as lesional is visibly higher within the actual lesions. In this step we threshold the density of voxels classified as lesional within a fixed adjacency radius, and consider lesional only those voxels with a density above a certain threshold, determined experimentally.

4. RESULTS

We used images from 5 epilepsy patients (age/gender: 11/M, 24/F, 12/M, 51/M, 30/F) with confirmed FCDs to evaluate the method. The lesions were manually segmented by an specialist with knowledge about the lesion locations, and this ground truth was used to extract a small training set of feature vectors from each patient. We used 1% of the voxels from each patient to build the training set, preserving a ratio of $1 : 9$ between lesional and healthy voxels. This ratio affects the radii of the RCE hyperspheres and can be used to control the ratio of false positives/false negatives in any direction.

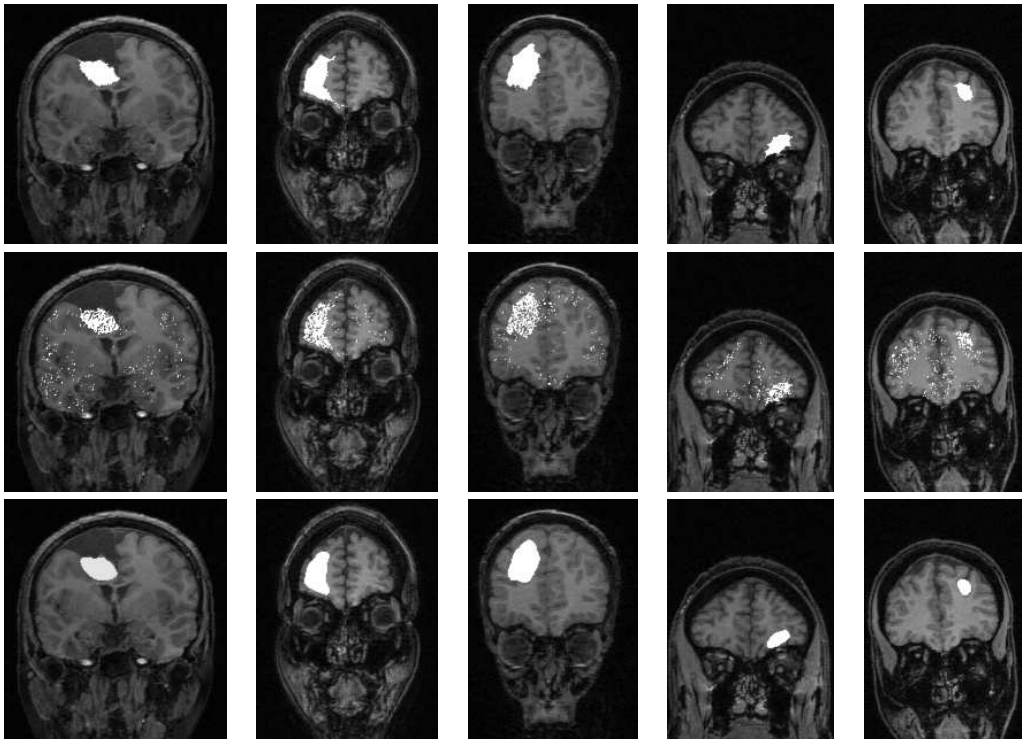

Fig. 2. Ground truth and segmentation results for the 5 patients. The first row shows the ground truth provided by an specialist. The second row shows the intermediary classification result. The third row shows the final classification result after the outlier removal step. Patients 1 and 3 are children, and patient 1 has a visible anatomical deformity (top left).

We used the *leave-one-out* scheme [20] to classify the voxels of each patient (each patient's voxels were classified using the training sets from the other four patients). We used a radius of 5 voxels and a density threshold of 35% for the outlier removal step. With these parameters, we detected all 5 lesions, with no false positives. The voxel coverage of the lesions ranged from 62.5% to 90.3% (average: 76.9%). Fig. 2 shows some sample slices of ground truth, intermediary classification (after step (v)) and final classification. Even though the intermediary classification appears clean on 2D slices such as those shown in Fig. 2, a 3D renderization shows that it contains too much noise. Fig. 3 shows 3D renderizations of the intermediary (a) and final (b) lesion segmentations for patient 2.

The lesion segmentation method took about 30 minutes per patient on an Athlon64 3200+ PC: 1 minute for MSP location (which includes the brain segmentation), 20 seconds for CR computation, 28 minutes for feature extraction and RCE classification, and 40 seconds for the outlier removal step.

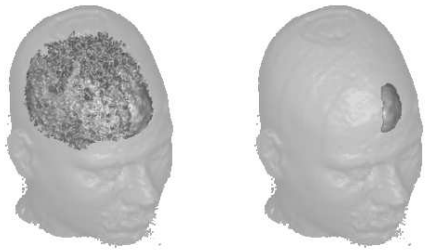

Fig. 3. 3D renderizations of the lesion segmentation for patient 2: (a) intermediary classification and (b) segmentation after outlier removal.

5. CONCLUSIONS

We presented a new method for segmentation of dysplastic lesions in MR-T1 images of the brain. Our method does not rely on template-based method and is applicable to any patient regardless of age or anatomical variations. We evaluated the method on 5 patients of ages 11y–51y, with good results on all of them. The average lesion coverage was 76.9%, providing a result slightly better than the state of the art [14].

Our method requires some adhoc parameters which were chosen experimentally, such as the radius and percentage values for outlier removal, and the parameters for texture features and RCE classifier training. We are currently working on automatic methods for choosing those parameters, as well

as measuring their effect on the segmentation results. We are also working on obtaining more datasets in order to validate the method in a larger set of patients.

6. REFERENCES

[1] D. C. Taylor, M. A. Falconer, C. J. Bruton, and J. A. Corsellis, "Focal dysplasia of the cerebral cortex in epilepsy," *J Neurol Neurosurg Psychiatry*, vol. 34, no. 4, pp. 369–387, Aug 1971.

[2] J. L. Frater, R. A. Prayson, H. H. Morris III, and W. E. Bingaman, "Surgical pathologic findings of extratemporal-based intractable epilepsy," *Arch Pathol Lab Med*, vol. 124, no. 4, pp. 545–549, Apr 2000.

[3] N. Colombo, L. Tassi, C. Galli, A. Citterio, G. Lo Russo, G. Scialfa, and R. Spreafico, "Focal cortical dysplasias: MR imaging, histopathologic, and clinical correlations in surgically treated patients with epilepsy," *Amer. J of Neuroradiology*, vol. 24, pp. 724–733, Apr 2003.

[4] P. M. Ruggieri, I. Najm, R. Bronen, M. Campos, F. Cendes, J. S. Duncan, H. G. Weiser, and W. H. Theodore, "Neuroimaging of the cortical dysplasias," *Neurology*, vol. 62, pp. S27–S29, 2004.

[5] A. Palmini, F. Andermann, A. Olivier, D. Tampieri, Y. Robitaille, E. Andermann, and G. Wright, "Focal neuronal migration disorders and intractable partial epilepsy: A study of 30 patients," *Annals of Neurology*, vol. 30, no. 6, pp. 741–749, Dec 1991.

[6] S. M. Sisodiya, "Surgery for malformations of cortical development causing epilepsy," *Brain*, vol. 123, no. 6, pp. 1075–1091, Jun 2000.

[7] S. Liu, N. An, H. Yang, M. Yang, Z. Hou, L. Liu, and Y. Liu, "Pediatric intractable epilepsy syndromes: Reason for early surgical intervention," *Brain & Development*, vol. 29, no. 2, pp. 69–78, Mar 2007.

[8] M. A. Montenegro, L. M. Li, M. M. Guerreiro, C. A. M. Guerreiro, and F. Cendes, "Focal cortical dysplasia: Improving diagnosis and localization with magnetic resonance imaging multiplanar and curvilinear reconstruction," *J Neuroimg*, vol. 12, no. 3, pp. 224–230, Jul 2002.

[9] A. C. Bastos, R. M. Comeau, F. Andermann, D. Melanson, F. Cendes, F. Dubeau, S. Fontaine, D. Tampieri, and A. Olivier, "Diagnosis of subtle focal dysplastic lesions: Curvilinear reformatting from three-dimensional magnetic resonance imaging," *Annals of Neurology*, vol. 46, no. 1, pp. 88–94, 1999.

[10] F. P. G. Bergo and A. X. Falcão, "Fast and automatic curvilinear reformatting of MR images of the brain for diagnosis of dysplastic lesions," in *Proc. 3rd Intl. Symp. on Biomed. Imaging*. Apr 2006, pp. 486–489, IEEE.

[11] J. Kassubek, H. J. Huppertz, J. Spreer, and A. Schulze-Bonhage, "Detection and localication of focal cortical dysplasia by voxel-based 3-D MRI analysis," *Epilepsia*, vol. 43, no. 6, pp. 596–602, Jun 2002.

[12] S. B. Antel, D. L. Collins, N. Bernasconi, F. Andermann, R. Shinghal, R. E. Kearney, D. L. Arnold, and A. Bernasconi, "Automated detection of focal cortical dysplasia lesions using computational models of their MRI characteristics and texture analysis," *NeuroImage*, vol. 19, no. 4, pp. 1748–1759, Aug 2003.

[13] S. Srivastava, F. Maes, D. Vandermeulen, W. van Paesschen, P. Dupont, and P. Suetens, "Feature-based statistical analysis of structural MR data for automatic detection of focal cortical dysplastic lesions," *NeuroImage*, vol. 27, no. 2, pp. 253–266, Aug 2005.

[14] O. Colliot, T. Mansi, N. Bernasconi, V. Naessens, D. Klironomos, and A. Bernasconi, "Segmentation of focal cortical dysplasia lesions on MRI using level set evolution," *NeuroImage*, vol. 32, no. 4, pp. 1621–1630, Oct 2006.

[15] D. L. Collins, A. P. Ziljdenbos, V. Kollokian, J. G. Sled, N. J. Kabani, C. J. Holmes, and A. C. Evans, "Design and construction of a realistic digital brain phantom," *IEEE Trans Medical Imaging*, vol. 17, no. 3, pp. 463–468, Jun 1998.

[16] M. B. Cuadra, C. Pollo, A. Bardera, O. Cuisenaire, J-G. Villemure, and J-P. Thiran, "Atlas-based segmentation of pathological MR brain images using a model of lesion growth," *IEEE Trans Medical Imaging*, vol. 23, no. 10, pp. 1301–1314, Oct 2004.

[17] F. P. G. Bergo, G. C. S. Ruppert, L. F. Pinto, and A. X. Falcão, "Fast and robust mid-sagittal plane location in 3D MR images of the brain," in *Proc. BIOSIGNALS 2008 – Intl. Conf. on Bio-Inspired Syst. and Sig. Proc.*, Jan 2008, pp. 92–99.

[18] F. P. G. Bergo, A. X. Falcão, P. A. V. Miranda, and L. M. Rocha, "Automatic image segmentation by tree pruning," *J Math Imaging and Vision*, vol. 29, no. 2–3, pp. 141–162, Nov 2007.

[19] R. Haralick, K. Shanmugam, and I. Dinstein, "Texture parameters for image classification," *IEEE Trans. Syst. Man Cyb. 3*, pp. 610–621, 1973.

[20] R. O. Duda, P. E. Hart, and D. G. Stork, *Pattern Classification*, Wiley-Interscience, 2nd edition, 2000.